# Aerial Measuring System Sensor Modeling

**Rebecca Detwiler, PhD**
**Bechtel Nevada**
**P.O. Box 98521, M/S RSL-24**
**Las Vegas, NV 89193-8521**
**702-295-8613**

This project deals with the modeling the Aerial Measuring System (AMS) fixed-wing and rotary-wing sensor systems, which are critical U.S. Department of Energy's National Nuclear Security Administration (NNSA) Consequence Management assets. The fixed-wing system is critical in detecting lost or stolen radiography or medical sources, or mixed fission products as from a commercial power plant release at high flying altitudes. The helicopter is typically used at lower altitudes to determine ground contamination, such as in measuring americium from a plutonium ground dispersal during a cleanup. Since the sensitivity of these instruments as a function of altitude is crucial in estimating detection limits of various ground contaminations and necessary count times, a characterization of their sensitivity as a function of altitude and energy is needed. Experimental data at altitude as well as laboratory benchmarks is important to insure that the strong effects of air attenuation are modeled correctly. The modeling presented here is the first attempt at such a characterization of the equipment for flying altitudes.

The sodium iodide (NaI) sensors utilized with these systems were characterized using the Monte Carlo N-Particle code (MCNP) developed at Los Alamos National Laboratory. For the fixed wing system, calculations modeled the spectral response for the 3-element NaI detector pod and High-Purity Germanium (HPGe) detector, in the relevant energy range of 50 keV to 3 MeV. NaI detector responses were simulated for both point and distributed surface sources as a function of gamma energy and flying altitude. For point sources, photopeak efficiencies were calculated for a zero radial distance and an offset equal to the altitude. For distributed sources approximating an infinite plane, gross count efficiencies were calculated and normalized to a uniform surface deposition of 1 $\mu Ci/m^2$.

The helicopter calculations modeled the transport of americium-241 ($^{241}Am$) as this is the "marker" isotope utilized by the system for Pu detection. The helicopter sensor array consists of 2 six-element NaI detector pods, and the NaI pod detector response was simulated for a distributed surface source of $^{241}Am$ as a function of altitude.

## Description of Gamma Sources Modeled

### *Point Sources*

Due to the large source-to-detector distances and the desire for a simulated detector response as a function of energy, the sources were directionally biased. This method was tested with calculations made with no directional biasing at an altitude of 100 meters (m), and photopeak results agreed within the statistical errors. As shown later in the paper, gross counts also agreed within errors with experimental data up to an altitude of

1000 feet (ft), although further work is needed to investigate discrepancies above that altitude. To minimize running time by not repeating close energies, a simulated gamma spectrum of spaced energies was used to express photopeak counts as a function of gamma energy. Energies ranged from 300 keV to 3 MeV for most fixed-wing altitudes. Point sources were modeled at two radial distances, one of zero radial distance with respect to the fixed-wing pod, and one at an offset radial distance equal to the altitude.

***Distributed Ground Sources***

The distributed sources were modeled after a uniform infinite plane surface distribution. In practice, a surface circular source of radius equal to the altitude was used for the fixed wing due to very low statistics from inadequate biasing ability for the distributed source. For fixed-wing distributed sources, a simulated gamma spectrum was also used, while only $^{241}$Am was used for the helicopter. Helicopter distributed sources were also modeled initially with the radius equal to the altitude. Additional runs were made at the lowest two altitudes for distributed sources with larger radii. Directional biasing was limited to biasing in the upper hemisphere for distributed sources.

**Modeling Environment**

The fixed-wing and helicopter systems were modeled above a 200m layer of earth with composition given by ANSI 6.6.1-1987 and inside a hemisphere of air with a 1000m radius. A density of 1.25E-3 g/cc was used for the air, 3.67g/cc for NaI crystals, and 5.3234g/cc for the HPGe crystal. The body of the fixed-wing aircraft was simplified to an aluminum sphere containing the detector pods.

**Detector and Pod Modeling**

The detector response as a function of energy was modeled for both the NaI and HPGe detectors, and photopeak counts were recorded from the generated spectra for the point sources. Although the Gaussian smoothing function added to the tally gives a more realistic detector energy response function, the results of counts in the energy bin containing the gamma photopeak energy with no Gaussian smoothing are identical to those obtained by summing the energy bins of the photopeak with Gaussian smoothing. Therefore, for photopeak calculations, spectra did not have the Gaussian function added, although the sample spectra shown later do have Gaussian smoothing.

***Fixed Wing***

Both a NaI pod and HPGe detector were modeled for the fixed-wing system. The NaI pod contained 3 NaI detectors. The detectors were housed in foam inside the fiberglass box, and were shielded with a thin layer of aluminum. The foam, fiberglass, and aluminum shielding were all modeled, using typical densities for the packing foam and fiberglass. The HPGe detector was modeled in foam inside a fiberglass case with a plastic cover.

***Helicopter***

The NaI pod, containing six NaI detectors aligned symmetrically about the center with three on each side, was modeled for the helicopter. Detection ends pointed toward the pod center and photomultipliers were at the opposite ends. The aluminum helicopter pod was simplified to a uniform layer. Again, the aluminum shielding around the NaI crystals and the packing foam were included in the modeling, as was a thin cadmium shield directly above the detectors.

## Benchmark Measurements

The benchmark measurements recorded spectra from a single detector for both the fixed-wing pod and helicopter pod and results were compared with MCNP calculations. For the fixed-wing pod, measurements were made for the larger NaI detector inside the pod, with the pod pointing head on and at 90° from the source at 1 m, for $^{241}$Am, cesium-137 ($^{137}$Cs), and cobalt-60 ($^{60}$Co) sources. The middle-sized detector was measured for one source, $^{137}$Cs, at the 90° orientation only. Photopeak counts were compared to calculated values. The helicopter benchmark was made with the pod mounted on the helicopter, at 90° from a source centered with respect to the right outer NaI crystal, approximately 1m below the crystal used. Sources used were $^{241}$Am, $^{137}$Cs, and sodium-22 ($^{22}$Na), and both photopeak and gross counts were compared. Refer to Table 1 and Table 2.

**Table 1. Benchmark Measurements and Calculations for Fixed Wing**

| **NaI Detector – Large** | | | | | |
|---|---|---|---|---|---|
| | | 90° Orientation | | 0° Orientation | |
| Isotope | Energy | Exp | MCNP | Exp | MCNP |
| $^{241}$Am | 0.05963 | 2.81E-03 | 2.34E-03 | 7.10E-04 | 6.21E-04 |
| $^{137}$Cs | 0.662 | 1.18E-03 | 1.31E-03 | 2.14E-04 | 1.74E-04 |
| $^{60}$Co | 1.1173 | 7.69E-04 | 8.40E-04 | 1.56E-04 | 1.394E-04 |
| | 1.332 | 6.01E-04 | 7.44E-04 | 9.90E-05 | 1.31E-04 |
| **NaI Detector – Medium** | | | | | |
| $^{137}$Cs | 0.662 | 3.26E-04 | 3.22E-04 | | |

**Table 2. Benchmark Measurements and Calculations for Helicopter**

| Outer NaI Detector | | | | | |
|---|---|---|---|---|---|
| | | Photo-Peak Efficiencies | | Gross Count Efficiencies | |
| Isotope | Energy | Exp | MCNP | Exp | MCNP |
| $^{241}$Am | 0.05963 | 2.5E-3 | 3.07E-03 | 2.70E-03 | 3.54E-03 |
| $^{137}$Cs | 0.662 | 1.53E-3 | 1.50E-03 | 5.32E-3 | 5.09E-03 |
| $^{22}$Na | 1.275 | 8.74E-04 | 8.76E-04 | 1.33E-02 | 1.42E-02 |

## Results and Analysis

The output of the MCNP detector response tally of counts per energy bin was given in counts per source gamma. These results were then normalized to appropriate measurable quantities. For the photopeak counts from the point source, the counts were normalized to a source strength of 1 μCi, giving a count rate in counts/s per 1 μCi. For the distributed sources, the gross counts were normalized to gross counts per second for the entire area of the surface deposition for a 1 μCi/m$^2$ deposition, or

(Gross Counts / ?) x (1?/d) x ((3.7e4 d/s)/ μCi) x (1 μCi/m$^2$) x Area(m$^2$) = (Counts/s) / (μCi/m$^2$)

The gross count rate per 1 μCi/m$^2$ at altitude can then be normalized to the dose rate mRem/hr or exposure rate mR/hr at 1m above ground level (AGL) from the count rate-energy curves shown in Figures 10 – 13 and appropriate exposure rate or dose rate conversion factors given in Table 3.4 of the *FRMAC Assessment Manual* [1]. The manual gives dose rates and exposure rates for a 1 μCi/m$^2$ infinite plane surface deposition evaluated at 1m AGL for a particular isotope. As the results here are for a mono-energetic source, the count rates at the appropriate energies corresponding to the gamma lines of the isotopes must be multiplied by the branching ratios and then summed. The resulting total count rate for the isotope at the given altitude per μCi/m$^2$ deposition must then be divided by the isotope's conversion factor from Table 3.4 to give the gross count rate at altitude for that isotope per unit dose or exposure rate at 1m AGL.

The following example illustrates the above method for the $^{60}$Co isotope at 1000 ft. At this altitude, the gross count rates at 1.173 MeV and 1.332 MeV are roughly 2.1E+1counts/s and 2.4E+1 counts/s, and the branching ratio for each is 1, giving a total

count rate for 1 µCi/m$^2$ $^{60}$Co deposition of (2.1E+1)x1 + (2.4E+1)x1 = 4.5E+1 (counts/s) / (µCi/m$^2$ ). The gross count rate at 1000 ft normalized to the EDE (effective dose equivalent) rate at 1m AGL would then be [4.5E+1(counts/s) / (µCi/m$^2$)] / [2.2E-2(mRem/hr) / (µCi/m$^2$)] = 2.05E+3 (counts/s) / (mRem/hr).

**Results for Fixed-wing Point Sources**

The point source modeling results for the fixed-wing aircraft are shown below. Photopeak efficiencies are shown separately for each of the three NaI detectors. Due to time constraints, many of the runs were not long enough to allow counts in the small 1"x1"D NaI detector. Figures 1–5 show results for point sources with zero radial distance from the center of the fixed-wing pod, while Figures 6–9 show results with a radial offset equal to the altitude. Figures 2-5 and 6-9 show the photopeak efficiencies for a point source strength of 1 µCi as a function of energy for the simulated gamma spectra used, while Figure 1 shows the efficiencies as a function of altitude for one point source, $^{137}$Cs. The results show the effects of air attenuation at distances larger than 100m in the drop off of efficiencies faster than the 1/r$^2$ dependence. The energy curves also show attenuation effects in a greater efficiency at higher energies for distances larger than 100m.

**Figure 1. MCNP Photopeak Efficiency as a Function of Altitude for $^{137}$Cs**

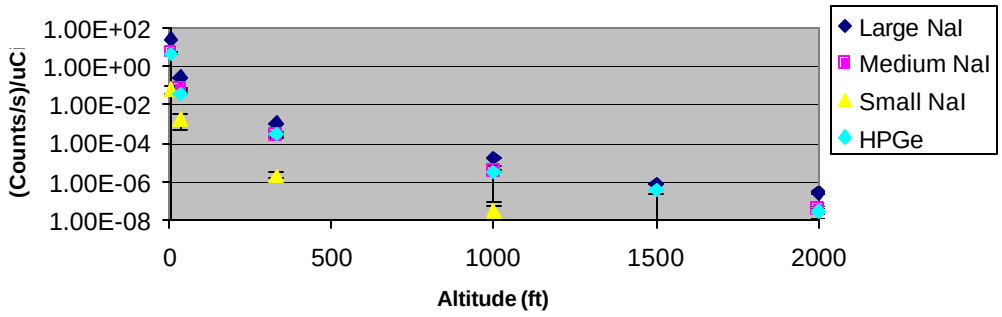

## Zero Radial Distances

**Figure 2. Photopeak Efficiencies for a Point Source at 328 ft (100 m)**

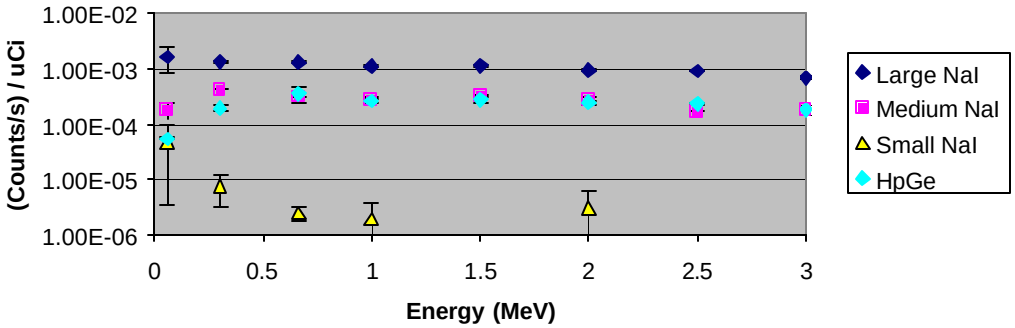


**Figure 3. Photopeak Efficiencies for a Point Source at 1000 ft**

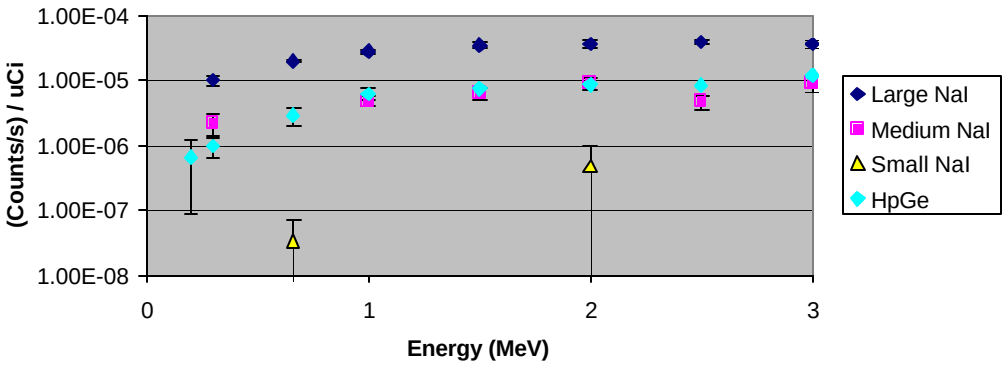

## Zero Radial Distances (continued)

**Figure 4. Photopeak Efficiencies for a Point Source at 1500 ft**

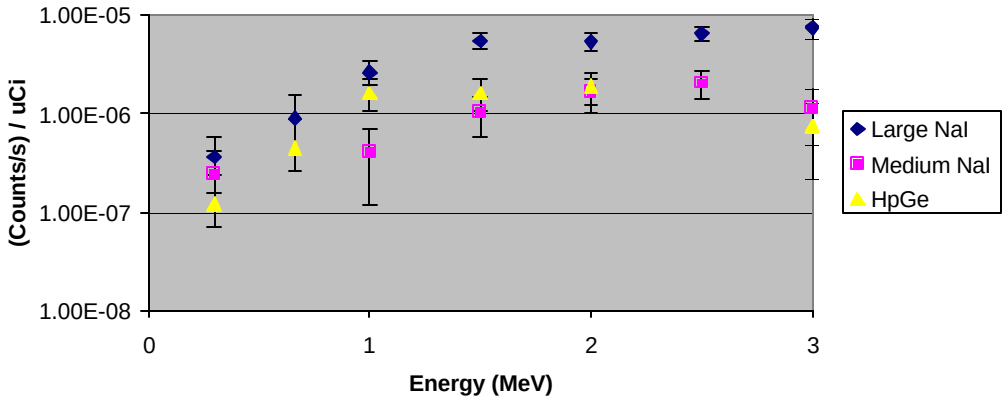


**Figure 5. Photopeak Efficiencies for Point Source at 2000 ft**

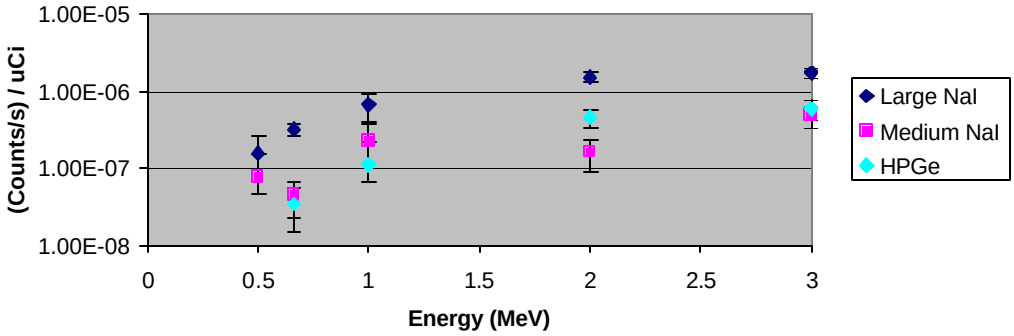


## Offset Radial Distances

**Figure 6. Photopeak Efficiencies for Offset Point Source at 328 ft (100 m)**

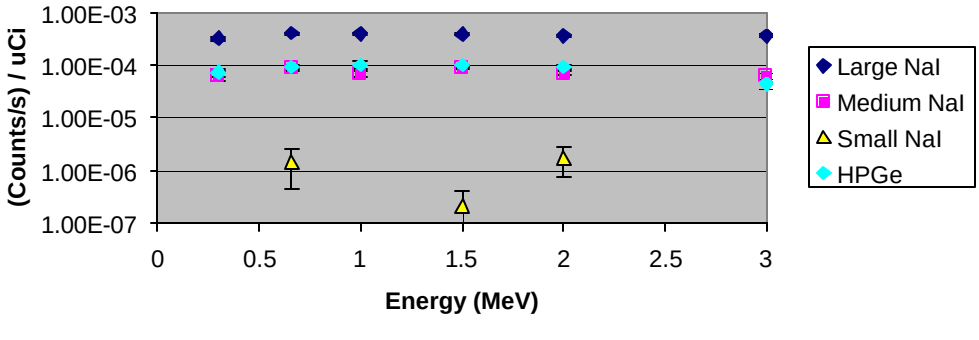

**Offset Radial Distances (continued)**

**Figure 7. Photopeak Efficiencies for Offset Point Source at 1000 ft**

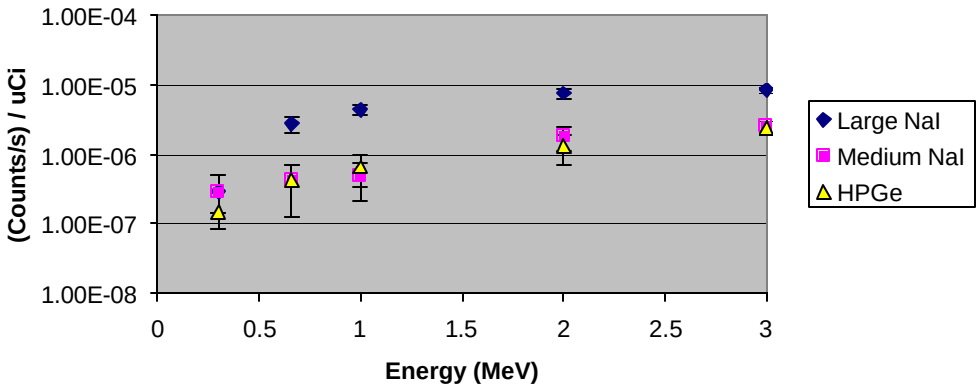


**Figure 8. Photopeak Efficiencies for Offset Point Source at 1500 ft**

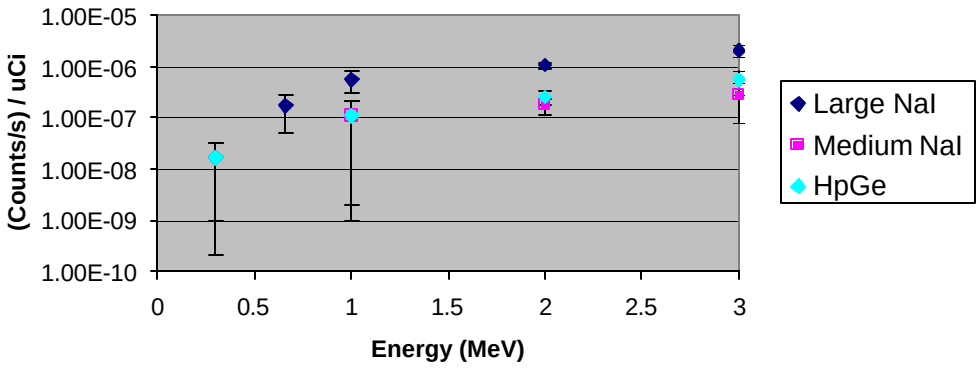


**Figure 9. Photopeak Efficiency for Offset Point Source at 2000 ft**

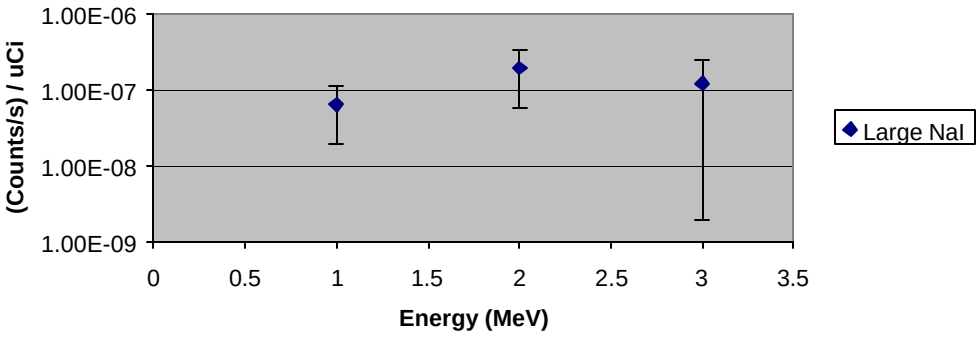

**Comparison to Data**

Figures 10 and 11 show a comparison of fixed-wing data to real data for an iridium-192 ($^{192}$Ir) source. Gross count rate for the large NaI detector is shown. The data and calculations at 500 and 1000 ft are not far off (30% and 10%), although the altitudes above 1000 ft show a drop off of calculations compared to the data. This is not explained by the expected air attenuation based air absorption at this energy, which with the distance change predicts a value at 1500 ft of roughly 30% that at 1000 ft. The sharper drop of Figure 10 as compared with Figure 11 above 1000 ft may be explained by lower representation of Compton scattering at smaller angles from the source due to stronger source directional biasing. However, reducing the biasing above that of the runs shown for Figure 11 does not seem to show an appreciable increase in gross count rate.

However, the photopeak efficiencies do follow to at least a factor of 2 or better the expected drops due to air attenuation and distance. Figure 12 shows the MCNP results for the 0.662 keV energy of $^{137}$Cs compared to the calculated drop-offs from the 1m value due to the $1/r^2$ drop and air attenuation. A value of 0.0028/m was assumed for the air attenuation coefficient $(\mu)^2$.

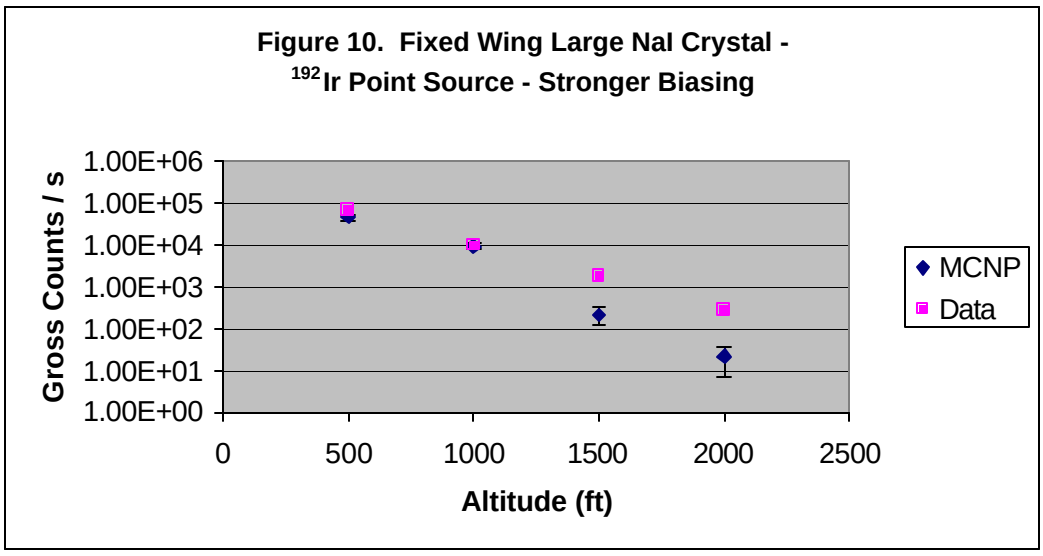

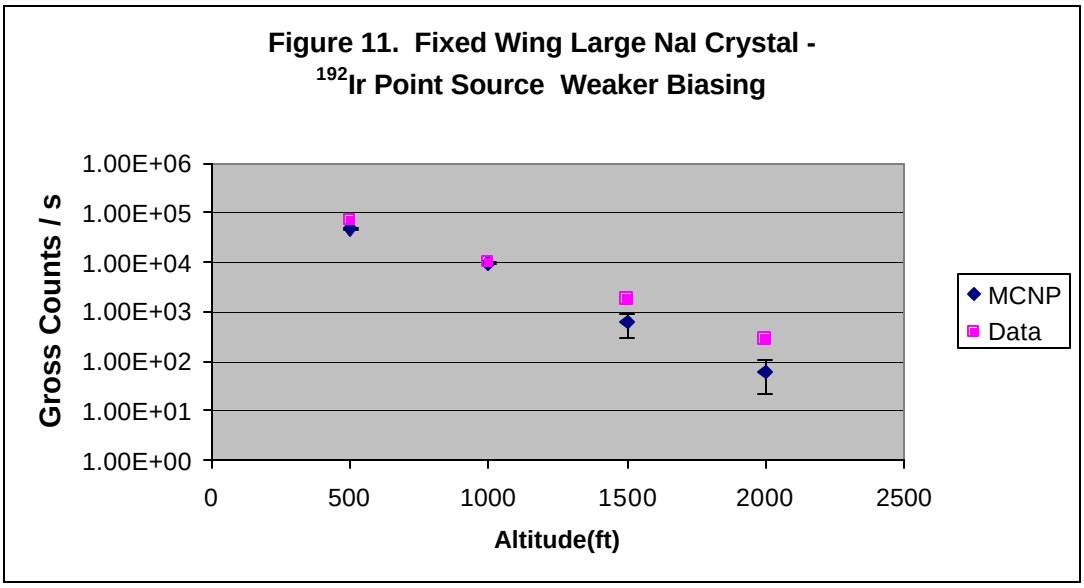


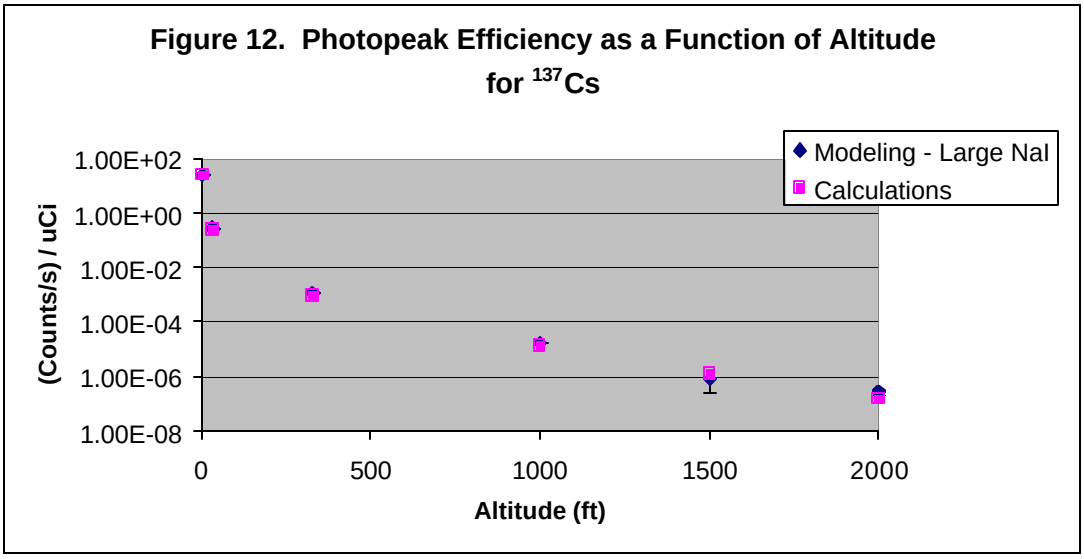


**Results for Fixed-Wing Distributed Sources**

The results for the fixed-wing distributed sources for are shown in Figures 13 – 16. As noted, they are uniform, circular surface sources approaching an infinite plane, with the radius equal to the altitude. Results of gross count rates are shown for the three sizes of NaI crystals, as well as for the HPGe detector. Counts were seen in the small circular 1"x1"D NaI detector only for the 100 m (328 ft) and 1000-ft altitudes. Error bars for the 1"x1"D NaI and HPGe detectors and other detectors at low energy points were cut off in several graphs to show the rest of the data more effectively. The count rates normalized to 1 $\mu Ci/m^2$ are shown for four altitudes of 100 m (328 ft), 305 m (1000 ft), 457 m (1500 ft), and 610 m (2000 ft).

**Figure 13. Gross Count Rate for 1uCi/m2 Deposition at 328 ft (100 m)**

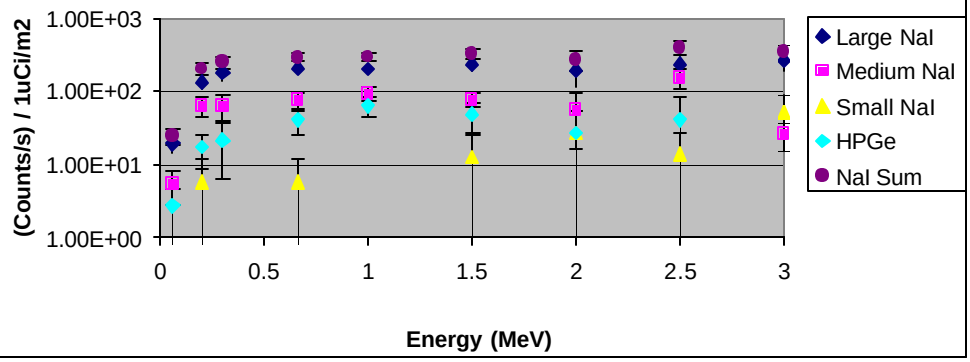


**Figure 14. Gross Count Rate for a 1 uCi/m2 Deposition at 1000 ft**

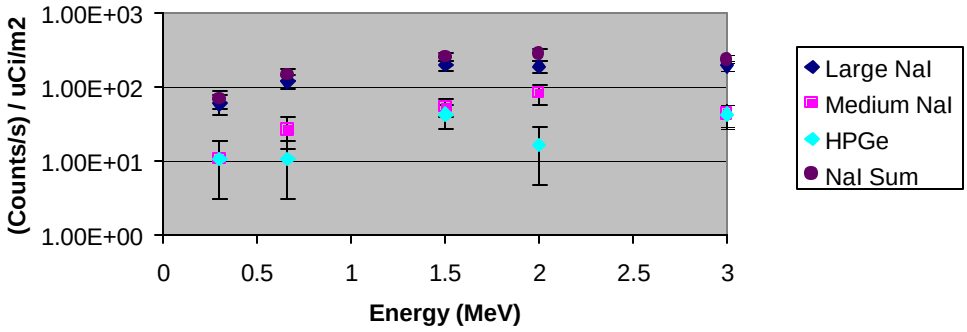


**Figure 15. Gross Count Rate for a 1uCi/m2 Deposition at 1500 ft**

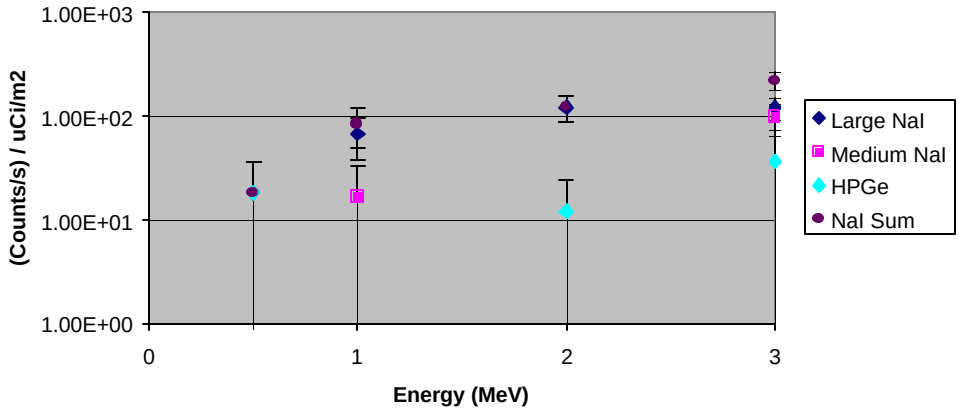

**Results for Distributed Sources (continued)**

**Figure 16. Gross Count Rate for a 1uCi/m2 Deposition at 2000 ft**

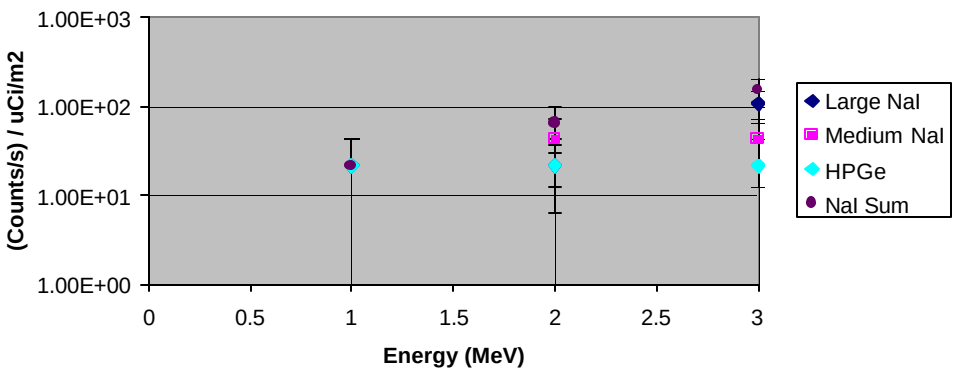


**Results for Helicopter**

The calculations for the helicopter, as previously stated, are made for a $^{241}$Am distributed surface source and are shown as count rate for one NaI pod normalized to a deposition of 1 µCi/m$^2$ as with the fixed-wing distributed sources. The distributed source was circular as before, with the radius equal to the altitude for the first graph, Figure 17. Altitudes were 50 ft, 150 ft, 300 ft, and 500 ft. The final two graphs, Figures 18 and 19, show the count rates as a function of the radius of the distributed source for the lowest two altitudes of 50 ft and 150 ft, for a radius of 1x, 2x, 4x, and 8x the altitude. The results indicate that for an altitude of 50 ft, at a radius of 8x the altitude, the distributed source approaches an infinite plane, while at an altitude of 150 ft, a larger radius may be needed. Due to time constraints, similar runs were not made for the higher flying altitudes.

**Figure 17. Gross Count Rate and Photopeak Count Rate for one Helicopter Pod**

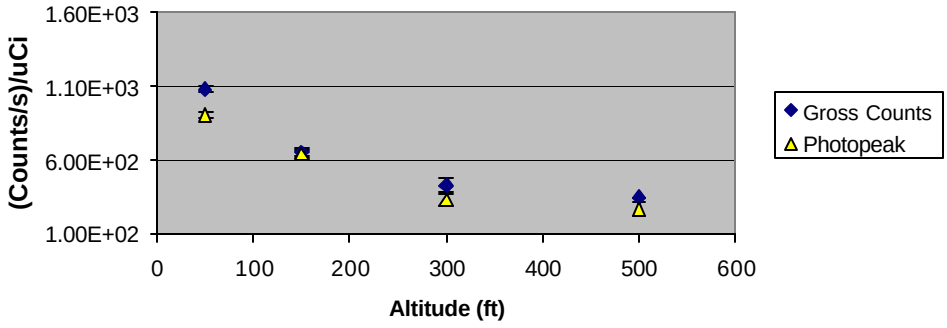

**Results for Helicopter (continued)**

**Figure 18. Heliopter Photopeak and Gross Count Rate as a Function of Radius of Distributed $^{241}$Am Source at 50 ft**

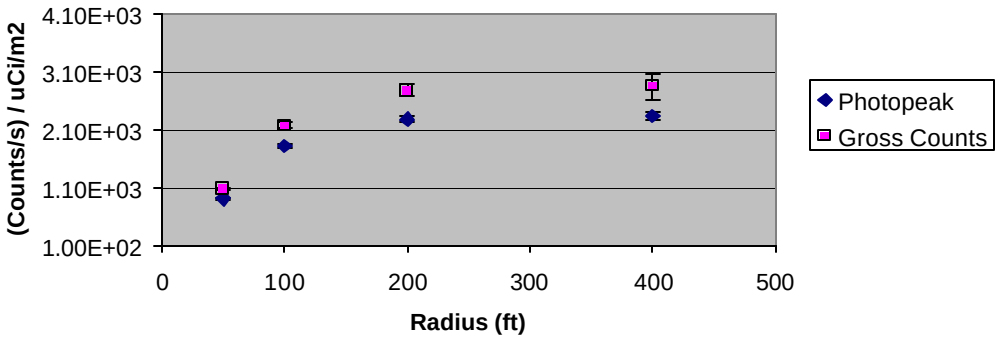


**Figure 19. Heliopter Photopeak and Gross Count Rate as a Function of Radius of Distributed $^{241}$Am Source at 150 ft**

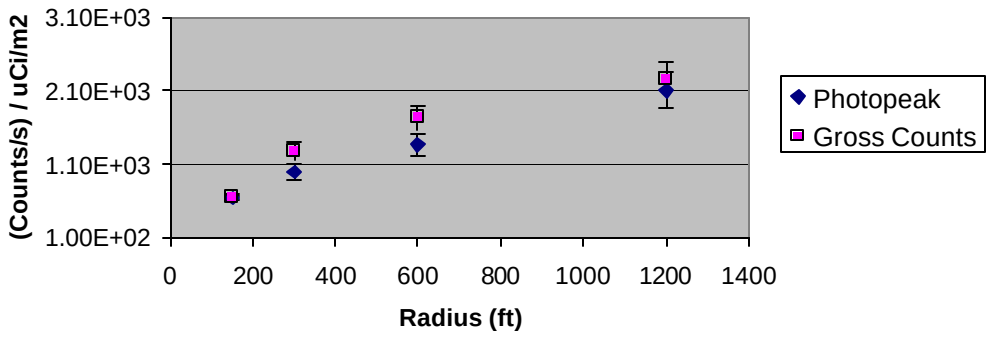


**Sample Fixed-Wing Spectra**

Figures 20 and 21 below show the spectra for HPGe and the largest NaI detector in the fixed-wing aircraft at an altitude of 328 ft (100 m) with no radial offset, while Figures 22 and 23 show the same spectra for an altitude of 1000 ft. Both have Gaussian broadening added to the tally, with 2.5keV Full Width Half Maximum (FWHM) for the HPGe spectra and 40 keV for the NaI spectra. The generation of spectra at altitudes of 1000 ft and greater was difficult due to low statistics in individual energy bins, as is shown in the spectra.

**Figure 20. HpGe Spectra for $^{137}$Cs at 328 ft (100 m)**

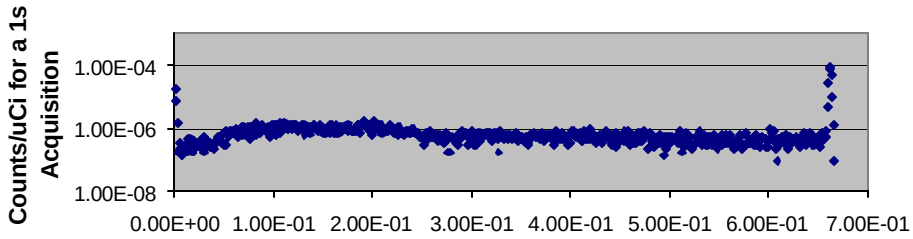


**Figure 21. Nal Spectra for $^{137}$Cs at 328 ft (100 m)**

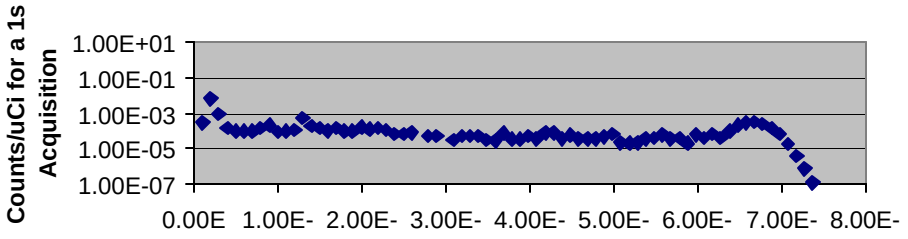


**Figure 22. HPGe Spectra for $^{137}$Cs at 1000 ft**

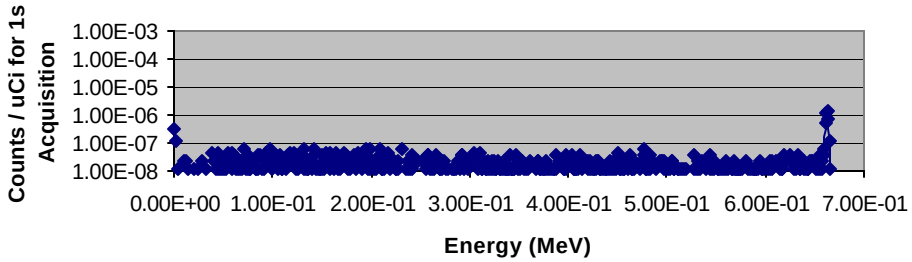


**Figure 23. Large Nal Spectra for $^{137}$Cs at 1000 ft**

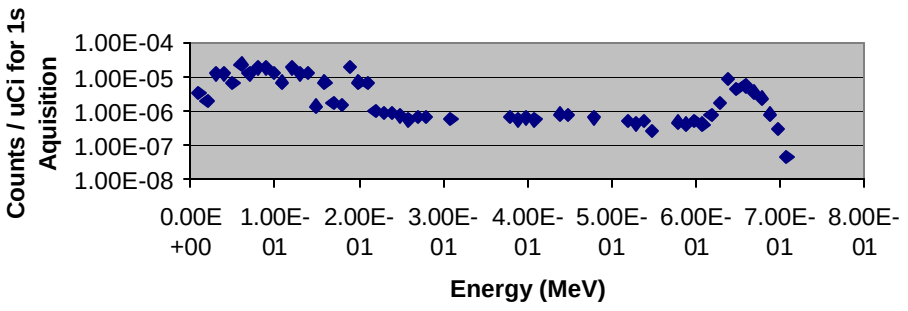

## Geometries

Figures 24 – 29 show the geometries of the detector pods that were modeled for the fixed-wing and helicopter systems.

**Figure 24. Fixed-wing NaI pod (blue) and HPGe pod (orange)- Vertical Cut**

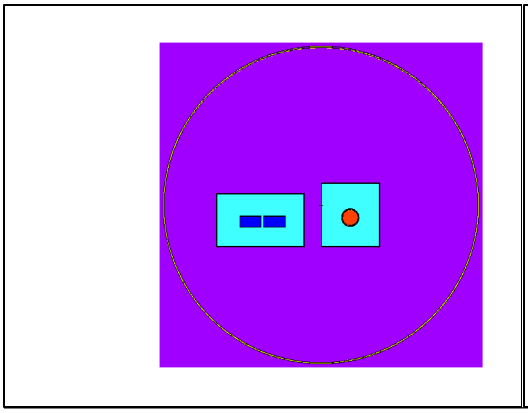

**Figure 25. Fixed-wing - Horizontal Cut**

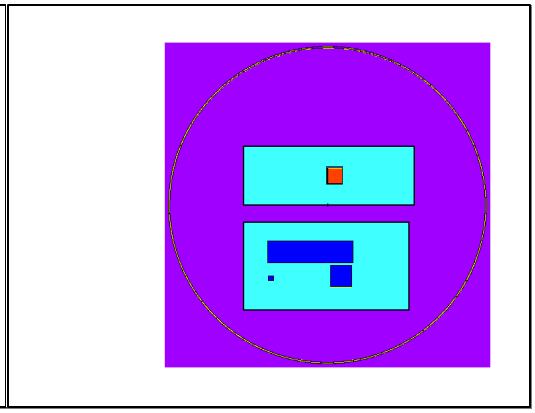

**Figure 26. NaI Pod Showing all 3 NaI detectors - Vertical Cut**

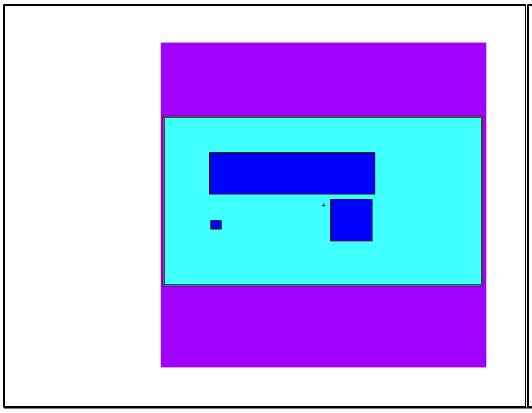

**Figure 27. NaI Pod with large and small NaI – Horizontal Cut**

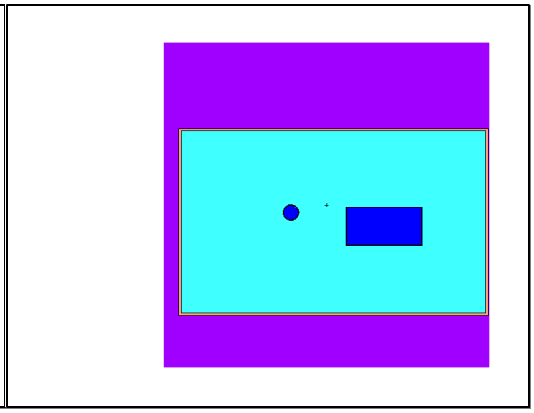

**Figure 28. Helicopter B200 Pod with 6 NaI detectors - Vertical Cut**

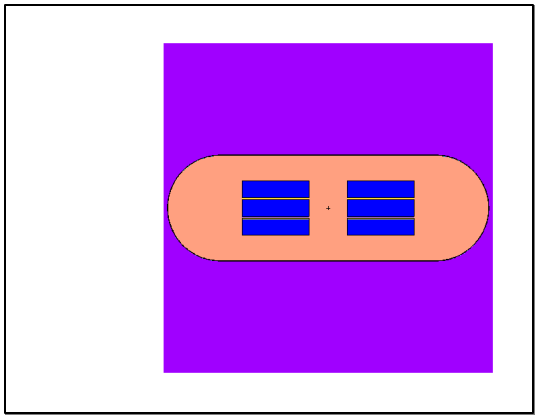

**Figure 29. Helicopter Pod - Horizontal Cut**

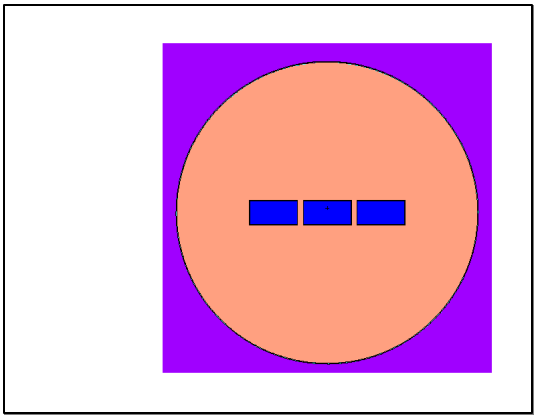

## Conclusion

These results represent the first attempt to model the AMS systems at flying altitudes using MCNP. As the comparison to data shows, the gross count results appear to be reliable up to 1000 feet. However, a problem with the model at higher altitudes will require more investigation. Clearly more data points are needed for comparison of fixed-wing photopeak efficiencies, gross counts at other energies, as well as the helicopter modeling.

Another difficulty to be addressed in future work is the poor statistics of the modeling. This is both due to poor transport caused by the air attenuation at the large distances (especially for lower energies) and inability to generate enough photons in a reasonable running time. While the results for the lower altitudes for the fixed-wing and helicopter results show fairly good statistics and number of data points, the modeling data for higher altitudes, especially for the distributed sources, suffers from low statistics and few data points at lower energies. Future endeavors will include developing a method for directional biasing of a large distributed source, and investigating other methods to speed calculations while retaining accuracy for both photopeak and gross count rate.

Additionally, the modeling could be improved by better estimates of the effective thickness of the fixed-wing aircraft, as the detector pods are inside the aircraft rather than outside, as with the helicopter.

## Bibliography


1. *FRMAC Assessment Manual*, Volume 2, U.S. Department of Energy, Las Vegas, NV, 1996.
2. *Radiological Health Handbook*, edited by U.S. Bureau of Radiological Health, 1970.



This work was supported by the U.S. Department of Energy, National Nuclear Security Administration Nevada Operations Office, under Contract No. DE-AC08-96NV11718.
**DOE/NV/11718—709.**